

# A comparative evaluation of strain measurement techniques in reinforced concrete structures—A discussion of assembly, application, and accuracy

Felix Clauß  | Mark Alexander Ahrens  | Peter Mark 

Institute of Concrete Structures, Faculty of Civil and Environmental Engineering, Ruhr University Bochum, Bochum, Germany

## Correspondence

Felix Clauß, Institute of Concrete Structures, Faculty of Civil and Environmental Engineering, Ruhr University Bochum, Universitätsstraße 150, 44801 Bochum, Germany.  
Email: felix.clauss@rub.de

## Funding information

Deutsche Forschungsgemeinschaft, Grant/Award Number: 398216472

## Abstract

The measurement of strain in structural elements is a necessary means of investigating the condition of a structure, both in research and in practice. The measurement methods for recording strain considered in this work represent both well-established techniques (strain gauges), as well as techniques that are part of rather current research streams (fiber optic sensors, digital image correlation). This work's contribution lies in providing an overarching comparison of these approaches, thereby informing practitioners and researchers as to parameters concerning their assembly, application, and their accuracy. To such ends, two test series were carried out, one on RC tension rods and another on a RC beam in a four-point bending test. From the latter scenario, for example, certain generalizations were to be deduced for varying load levels: low strains are measured well using the fiber optic technique. Conversely, digital image correlation was discovered to be an adequate choice when assessing higher strain levels and concomitant concrete cracking, as this non-contact technique avoids imprecisions caused by adhesives. Findings are to assist the future user by contrasting the three techniques in terms of assembly, handling, application and resilience of sensors, external influences as well as measurement resolution and accuracy. Such practice-oriented remarks should simplify a selection of the suitable measurement techniques catering to the respective, context-dependent testing scenario.

## KEYWORDS

accuracy, concrete, crack, digital image correlation, fiber optic sensors, measurement techniques, repeatability, strain, strain gauges

Discussion on this paper must be submitted within two months of the print publication. The discussion will then be published in print, along with the authors' closure, if any, approximately nine months after the print publication.

This is an open access article under the terms of the Creative Commons Attribution License, which permits use, distribution and reproduction in any medium, provided the original work is properly cited.

© 2021 The Authors. *Structural Concrete* published by John Wiley & Sons Ltd on behalf of International Federation for Structural Concrete.

## 1 | INTRODUCTION

Faced with an aging body of infrastructure,<sup>1</sup> for example, bridges are subject to constant changes in current standards, the field of structural health monitoring continues

to attract significant attention.<sup>2–5</sup> Within this domain, not only bridges,<sup>6–8</sup> but tunnels<sup>9</sup> get into the center of research attention. In this context, deformation, strain, and temperature<sup>10–12</sup> are often measured.

Rather recent developments in measurement technology (e.g.,<sup>13–18</sup>), such as the advent of fiber optic sensor (FOS) or digital image correlation (DIC), have opened up new avenues for research and practice. Said new devices constitute a significant addition to long-established measuring techniques. Among these, strain gauges have gained particular prominence in the past due to their ease of handling, high robustness, and high accuracy. When juxtaposing these three options for their efficacy and appropriateness in testing real structures,<sup>4</sup> questions as to their (ease of) handling, as well as their measurement resolution/accuracy arise (and are to be explored in this work). Influencing factors arising in field applications are in many cases even more extensive. Temperature changes as an example among a variety of environmental influences are often to be taken into account in measurements or even to be corrected.<sup>19</sup>

In addition to their use in practical scenarios, which are self-evidently particularly concerned with the respective technology's (ease of) applicability/handling, the three measuring techniques (FOS, DIC, strain gauges) are also suitable for detailed measurements under laboratory conditions. However, these often desired precise measurements up to the assumed exact measurement of quantities such as displacements or, in this case, strain, can suffer immensely different means and quality of application.

Influencing factors that are difficult to capture, for example, the quality of the bonding of sensor (strain gauges and FOS) and the respective surface or even the thickness of the adhesive layer, affect the measured results.

Recently, a significant volume of research has been carried out on the application of FOS<sup>20–22</sup> and DIC technology in reinforced concrete (RC) context.<sup>23</sup> Here, the focal point is set on optimizing and extending the ways in which these technologies are put to use—for example, improving the application of the measuring techniques (onto the testing object).

As an extension of the existing body of knowledge and in attempting to provide useful guidelines for differentiating between and selecting a technology, a comparative evaluation of the techniques' accuracy is needed. For this purpose, this work will primarily concentrate on measurements with the mentioned techniques in RC. In addition, occasional remarks on their application on pure steel, that is, a scenario with less influencing factors, are offered. Therefore, two test series were carried out – first on RC tension rods and secondly on an RC beam in a four-point bending test. On such basis, the results can be

used to derive practicable recommendations for the application of the respective measuring technique. Ensuingly, an explanation of various influencing factors ushers in the comparison of the accuracies of the different measuring techniques. Hence, recommendations for strain measurement are finally deduced.

## 2 | UNDERLYING PRINCIPLES OF STRAIN MEASUREMENT TECHNIQUES

### 2.1 | Strain gauges

Apart from displacement transducers in engineering-specific structural tests, strain gauges are the most frequently used measuring technique. Strain gauges (cf. Figure 1) consist of a wire laid in meanders on a carrier foil. When strain gauges are used to measure strain, the change in electrical resistance of the wire is measured. As this measuring technique has been established for years, we will refrain from describing it in detail. A more comprehensive discussion can be found in Reference 24.

### 2.2 | Fiber optic sensors

Fiber optic<sup>25–29</sup> devices permit the measurement of strain or temperature changes by evaluating the backscatter of an induced light beam in the fiber under test. Since the used fiber optic device (ODiSI-B, Luna Inc.) detects the Rayleigh backscattering, further explanations are limited to said share. The Rayleigh backscatter of an induced light beam, which is thus caused by the variable refractive index along the fiber, is recorded by detectors in the fiber optic device. This measurement is performed in the unloaded state, as well as during loading, as shown in Figure 2.

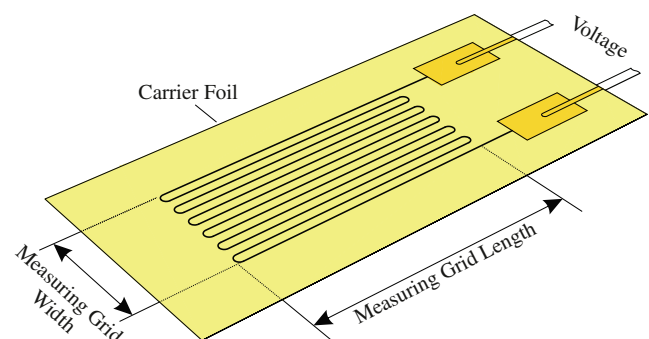
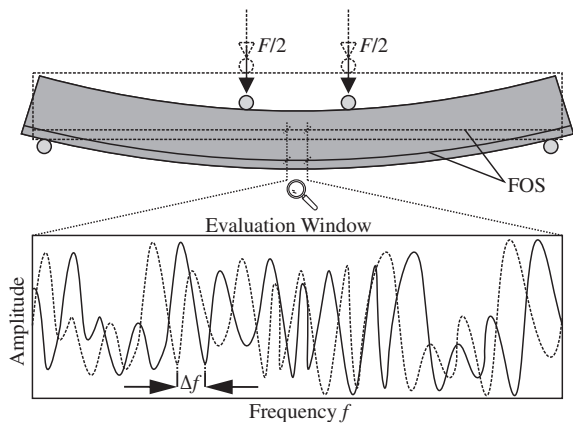


FIGURE 1 Principle Sketch of a Strain Gauge



**FIGURE 2** Measurement of a Frequency Shift  $\Delta f$  caused by Strain in a FOS (modified with reference to Claub, 2020)

This procedure results in two outgoing signals, that is, one for each scenario. Converted into frequency domain and then assessed in smaller evaluation windows (cf. Figure 2), the frequency shift  $\Delta f$  (unloaded vs. loaded) in an evaluation window can be directly related to both change in strain  $\Delta \varepsilon$  and temperature  $\Delta T$ , using the coefficients for strain  $K_\varepsilon$  or temperature  $K_T$  and the center wavelength  $l$  and the speed of light  $c$ .<sup>30,31</sup>

$$\Delta f = \Delta \varepsilon \cdot \left[ -\frac{c \cdot K_\varepsilon}{\lambda} \right] + \Delta T \cdot \left[ -\frac{c \cdot K_T}{\lambda} \right] \quad (1)$$

As specified in Equation (1), frequency shifts can be caused by a change in temperature, a change in strain, or both. Hence one of these influences must be kept constant or controlled by a second measurement.

### 2.3 | Digital image correlation

With DIC,<sup>32–35</sup> a displacement field of a surface can be calculated from juxtaposing detailed photos of a test specimen before and during different stages of loading. For this purpose, a preferably random speckle pattern is applied to the surface to be examined. As shown in Figure 3, the speckle pattern is then divided up into facets at pixel level. Each facet consists of matrices of  $n_x \times n_y$  gray tones—the center of each facet is thus assigned a unique set of gray tones. In turn, comparing images detected before and during loading, said facets form the basis for calculating displacements (of each facet) and finally strains for a meta area. In short, while an applied load deforms the test specimen, each facet undergoes movement from its initial position.<sup>36</sup>

The aim is to locate the set of gray tones from the unloaded state (reference facet) in each image during

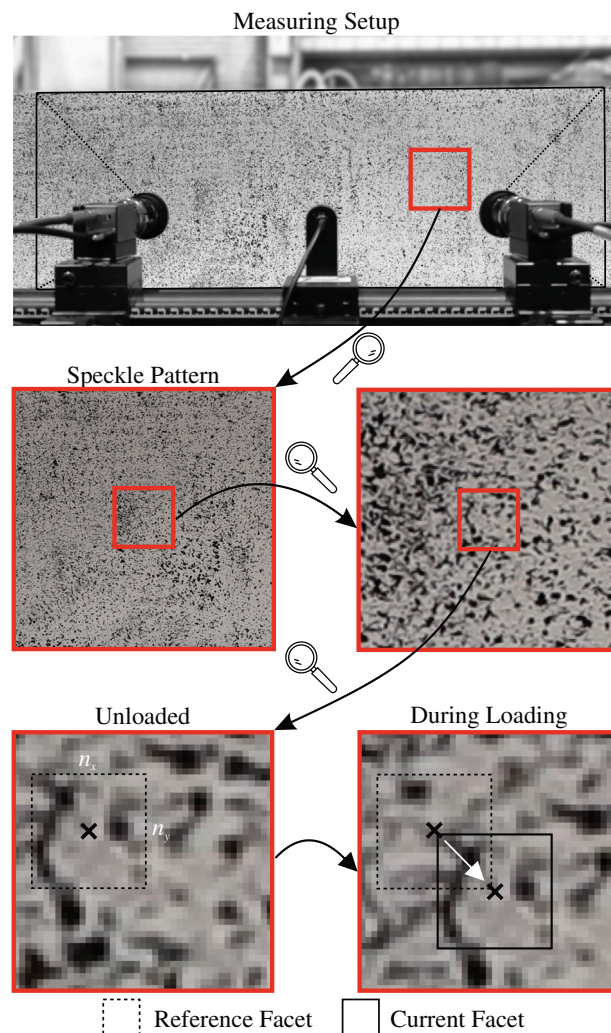


**FIGURE 3** Principle Strain Measurement of DIC (modified with reference to Claub, 2020)

loading. When strain is applied, each facet and thus its individual set of gray tones cannot only be shifted but also be rotated or experience slight modifications due to altered exposure to lighting. To reduce complexity, however, the facet shown in Figure 3 is only shifted.

By applying the least-squares method,<sup>37</sup> each facet center's displacement is determined. Using the deformation results from the immediate vicinity of each point, strain can be calculated for a meta area.

## 3 | EXPERIMENTS

### 3.1 | Tension rod

#### 3.1.1 | Test set-up

In a first test series, different types of fibers (FOS), as well as adhesives, were tested regarding their precise strain

measurement qualities in concrete structures. Tested were nine identically shaped RC tension rods with cross-sectional dimensions of 70 mm × 70 mm. As depicted in Figure 4, the test specimens, through which a reinforcement bar (1 Ø 12) passes centrally, exhibit a length of 550 mm. To apply load to the test specimens, the reinforcement bars—protruding 175 mm on both sides—were later clamped into the testing machine.

In order to predetermine the location of the initial damage, two notches in each of the concrete structures and reinforcement bars were prepared facing each other. These intended weak points were placed centrally of the longitudinal axis of the test specimens, and therefore the first crack in the concrete was to emerge right at this point. In addition to the two aforementioned ones, a notch along the entire reinforcement bar was added. Such modification rendered it possible to place the first of the two FOS within said notch, thereby enclosing and protecting it from heightened exposure to surrounding concrete. The other FOS was installed along the web of the reinforcement bar, that is, the exact opposite side of the bar. In this way, by comparing strain measurements produced by one enclosed and one non-enclosed FOS, the difference between both placements could be assessed.

Table 1 lists the examined adhesives and fibers. Generally, polyimide fibers and cyanoacrylate present common materials for fiber optic applications.<sup>38</sup> Besides, fibers with acrylate and titanium doped coatings were investigated. Especially the inevitably rough handling of the fiber itself during concreting motivates the test of a

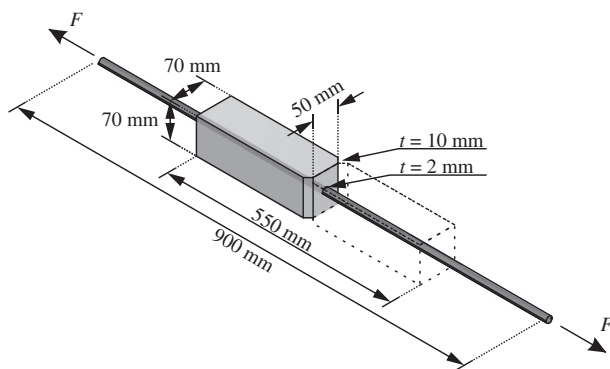


FIGURE 4 Test Set-Up of Tension Rods

stiffer fiber, that is, fiber with a titanium doped coating. In addition to a standard 5 min -epoxy resin, the AC2411 adhesive by Polytec PT was also investigated.

At a tensile strength of the concrete of approx. 4 N/mm<sup>2</sup>, according to Eurocode 2, the tensile force causing the theoretical first crack in the middle of the test specimen is 14 kN.

### 3.1.2 | Results

In the following, the selected results of the tests on the RC tension rods are presented in accordance with the objectives set for this work. Figure 5(a) shows the strain curves for a load of 5 kN, which corresponds to approximately 30% of the force required to produce the first crack at the, as described preset location at the center of the longitudinal axis of the rod.

For all three strain curves, it can be observed for the protrusions of the reinforcement, symmetrically on both sides of the rod, there are almost constant strain levels. The strain of approx. 230 µstrain measured here corresponds to the calculated strain in the rebar under the assumption of Hooke's law. In between the plateaus on each side, the stress detected in the reinforcement bar decreases due to the bonding behavior with the surrounding concrete. In a crack, however, the concrete's participation is interrupted abruptly.

Not all combinations of fiber type and adhesive are able to capture the steep course (large gradient) precisely. At this point, a distinction has to be made between different characteristics resulting from a soft or stiff adhesive and coating as follows. When using the cyanoacrylate adhesive, areas are identified where no strain can be measured ( $x = 130\text{--}180\text{ mm}$  and  $x = 650\text{--}710\text{ mm}$ ). Since this fiber optic measuring device can record strain gradients of approx. 150 µstrain of neighboring points, areas exceeding this limit are excluded from measurement entirely. One option to counteract such failure is to reduce the size of the evaluation window. A reduction in the size of the evaluation window, therefore, has the consequence that larger strain gradients can be recorded due to the finer resolution of the measurement.

The strain curve representing the standard epoxy resin displays similar characteristics. One notable

		Adhesive		
		Cyanoacrylate	Epoxy resin	AC2411
Coating	Polyimide	X	X	X
	Acrylate	X	X	X
	Titania 125–9	X	X	X

TABLE 1 Overview of investigations on RC tension rods with different fibers and adhesives

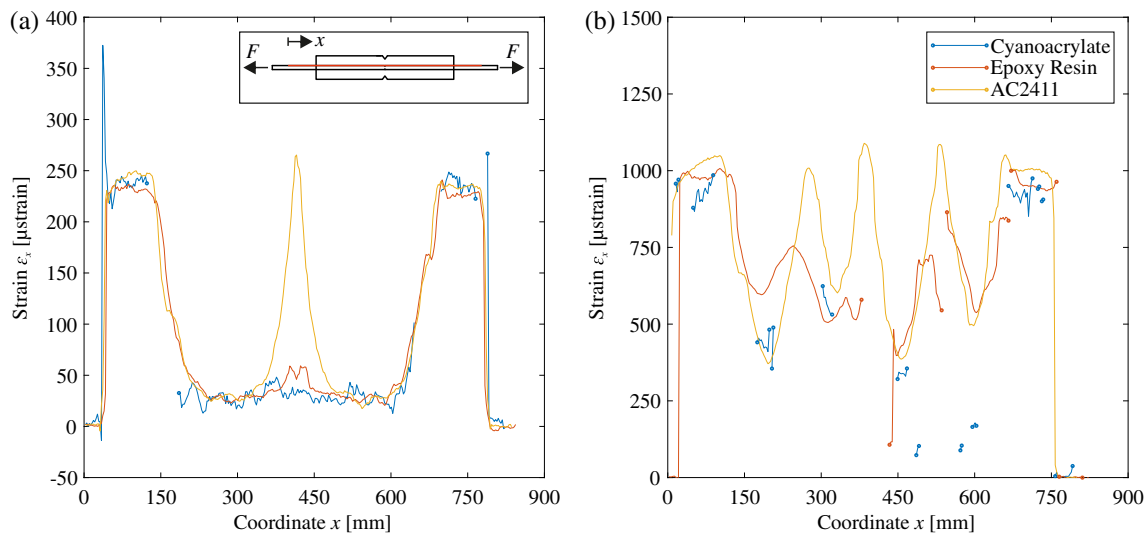


**FIGURE 5** Strain Measured by FOS Using Cyanoacrylate, Epoxy Resin and AC2411 at a Load Level of a)  $5 \text{ kN} = 0.30 F_{cr}$  and b)  $20 \text{ kN} = 1.30 F_{cr}$

exception is that strain results measured along their path are much smoother and continuous (without measurement failures). That is, the strain gradients between adjacent points do not exceed  $150 \mu\text{strain}$ . Furthermore, a slightly increased strain can be seen at the center longitudinal axis of the concrete structure, that is, notched area predetermined to crack first.

The results of the AC2411 adhesive features high similarities with the results of the standard epoxy resin. The main divergence is to be detected at the aforementioned location. Said difference occurs when a crack develops, the reinforcement in the axis of the crack takes over the force exerted upon it. The strain peak at the middle indicates the reinforcement beam's complete takeover of the acting force of approx.  $255 \mu\text{strain}$ . Due to the formation of a crack in merely one of the three test specimens shown, the strain in this area is no longer quantitatively comparable. The integration of the strain to a total elongation of the test specimen thus yields different values.

The tested cyanoacrylate adhesive exhibits a higher stiffness than the standard epoxy resin and AC2411. This characteristic conditions that strains are transferred into the fiber at the very point where they occur. This direct force transmission from the structure into the fiber allows for the most accurate and realistic results. Vice versa, as can be seen in the results of the epoxy resin and AC2411 adhesive, the strains are not directly transferred into the FOS but are first diffused by and transported via a larger area of the adhesive. Such spreading behavior, as displayed in Figure 5(a), results in a slight distortion of the results. Submitted to augmented levels of force, such a falsifying effect could increase drastically and, for example, cause a drop of the measured strain peak at the position of crack emergence. Hence, the adhesive's lack of stiffness not only

engenders a smoothing of the measured strain points at any load (e.g., compared cyanoacrylate) but, more importantly, corrupts the detection of peak strain measurements in areas of crack emergence in increased load scenarios. Here, said adhesives with lower stiffness would therefore condition a decrease in the detected strain at the crack itself and redistribute strain to and past the crack's shores—effectively a de-localization.

Figure 5(b) illustrates the strain results using the different adhesives for a load of 20 kN (i.e., approx.  $1.30 F_{cr}$ ). The measured strain peaks present in the midsection of the rod (between  $x = 225$  and  $550 \text{ mm}$ ) indicate several cracks in the concrete. Again, the force supposedly carried by the concrete is locally taken over by the reinforcing steel. In the scattered results of the cyanoacrylate, it can be seen that due to the increasing load and the associated progressive crack occurrence and growth, the limit value of  $150 \mu\text{strain}$  of adjacent strain results is often exceeded, and strain measurements for the rebar fail to a large extent. Such areas are likewise partially present in the depiction of results for the epoxy resin. Nevertheless, the course of both graphs suggests broadly similar strain measurements for said adhesives.

The variance in stiffness of the layer of adhesive around the FOS (as was detailed for various adhesives), therefore, always causes a spreading of the strain over immediately adjacent areas and slightly distorts the absolute measured values. The highest degree of smoothing and distortion thus occurs with AC2411, that is, the softest adhesive, followed by epoxy and cyano. AC2411 conversely, however, features the highest degree of continuity in measurements, that is, avoids measurement failures. Therefore, in theory, a trade-off between measurement accuracy and continuity, particularly

relevant in higher load scenarios, must be taken into account when selecting an adhesive. In practice, however, AC2411 clearly lends itself best to test set-ups with gradually increasing load levels.

Similar findings can be derived from comparing the results of glass fibers with different coatings (cf. Table 1). A rather soft layer around the glass fiber, as is the case for acrylate or titanium coating, also manipulates the measured strain levels. In a process parallel to the detailed behavior of differently stiff adhesives, this transfer of strain to surrounding areas rises with increasing load levels. Overall, observation of strain measured by FOS seems to be promising and of sufficient quality up to about  $1.3 F_{cr}$  as a rule of thumb. While  $1.0 F_{cr}$  is associated with the first crack of the specimen,  $1.3 F_{cr}$  characterizes a completed crack pattern with all primary cracks at regular distances. For loads above that level, an increasing smoothing and transfer of strains into adjacent regions happens due to the low stiffness of the adhesive. At higher loads, overlapping of impaired regions and must be taken into account.

## 3.2 | Four-point bending test

### 3.2.1 | Method of investigation

Now that the preliminary investigations for FOS have been carried out on one of the simplest structures, that is, tension rod, the next step is to increase the complexity of the system (test specimen under test) to obtain further results. The static system to be examined should satisfy various requirements. As such, the basic structure should allow for simple derivation of results and feature both compressive and tensile strains in the cross-section. Also, the specimen's characteristics as to spatial dispersion of the strain state over the height and the resulting moderate strain gradient should allow for optimal comparability of the strain measurement techniques. Precipitating from such requirements, the choice of the static system for this testing scenario is a single-span beam, which is loaded in a four-point bending test. The RC beam is successively loaded up to 160 kN, with the load levels being held at a constant level every 5 kN for a short period of time. By being able to assess the respective technique's measurements during such (temporarily) constant load levels as steady, the repeatability of the strain measurement techniques can be investigated.

### 3.2.2 | Test set-up

An RC beam of the dimensions of 150 mm/400 mm/2400 mm ( $b/h/l$ ) was concreted at Ruhr University Bochum.

The test specimen was tested in a four-point bending test with a span length of 2000 mm. The two concentrated loadings were placed right in the middle between the supports with a distance of 660 mm to each other (cf. Figure 6).

This loading scenario necessitates a bending reinforcement of 2  $\emptyset$  16 mm and stirrups  $\emptyset$  10 mm/20 cm/2. Additionally, a constructive reinforcement of 2  $\emptyset$  8 mm in the compressive zone was added. Excluded from the ensuing remarks on test set-up and arrangement of measurement technology in the test specimen are the ultrasonic transducers. As was discussed in earlier works,<sup>23</sup> they were installed, especially in the shear-free area between the point loadings. In order to position these ultrasonic transducers, the otherwise obsolete stirrups are also extended to the shear-free zone.

For better compaction, the beam was concreted on the side surface. This process offered the additional advantage of a smooth management of all sensors during concreting. This rather unusual concreting orientation is not expected to have any influence on the load-bearing behavior and thus on the strains investigated. But against the background of installing multiple measurement techniques, it made things much easier.

As detailed above, three different methods were employed for strain measurement. To reiterate, one can distinguish between standard strain gauges (SG), FOS, and DIC.

In order to ensure that the different technological (measuring) devices do not influence each other, their positioning was construed in a way limiting interference to a minimum. By means of an example, the cameras used for DIC collected imagery on one side of the RC beam, while FOS and SG were arranged on the other side of the body. The speckle pattern (DIC) is thus only applied to the front-side (cf. Figure 6 top and Figure 7) and captured by the cameras, which are placed at the shortest possible distance between them and the test specimen. This is to procure the highest possible pixel density (number of pixels per area), and therefore the highest possible information density for calculating surface strains while simultaneously avoiding a loss of camera focus. At such a distance, the maximum recordable width of the camera lenses employed here, 1000 mm, is fully exploited. Due to the fixed aspect ratio of the captured images, the height of the beam is also captured completely.

The FOS, by contrast, were attached to the back of the beam. In this experiment, the system ODISI-B of Luna Inc. was used and combined with an eight-channel fiber optic switch. Said switch permits the utilization of up to eight sensors in this test, however, only in (short) succession of one another. However, by means of suitable programming in C++ in the Software Development Kit

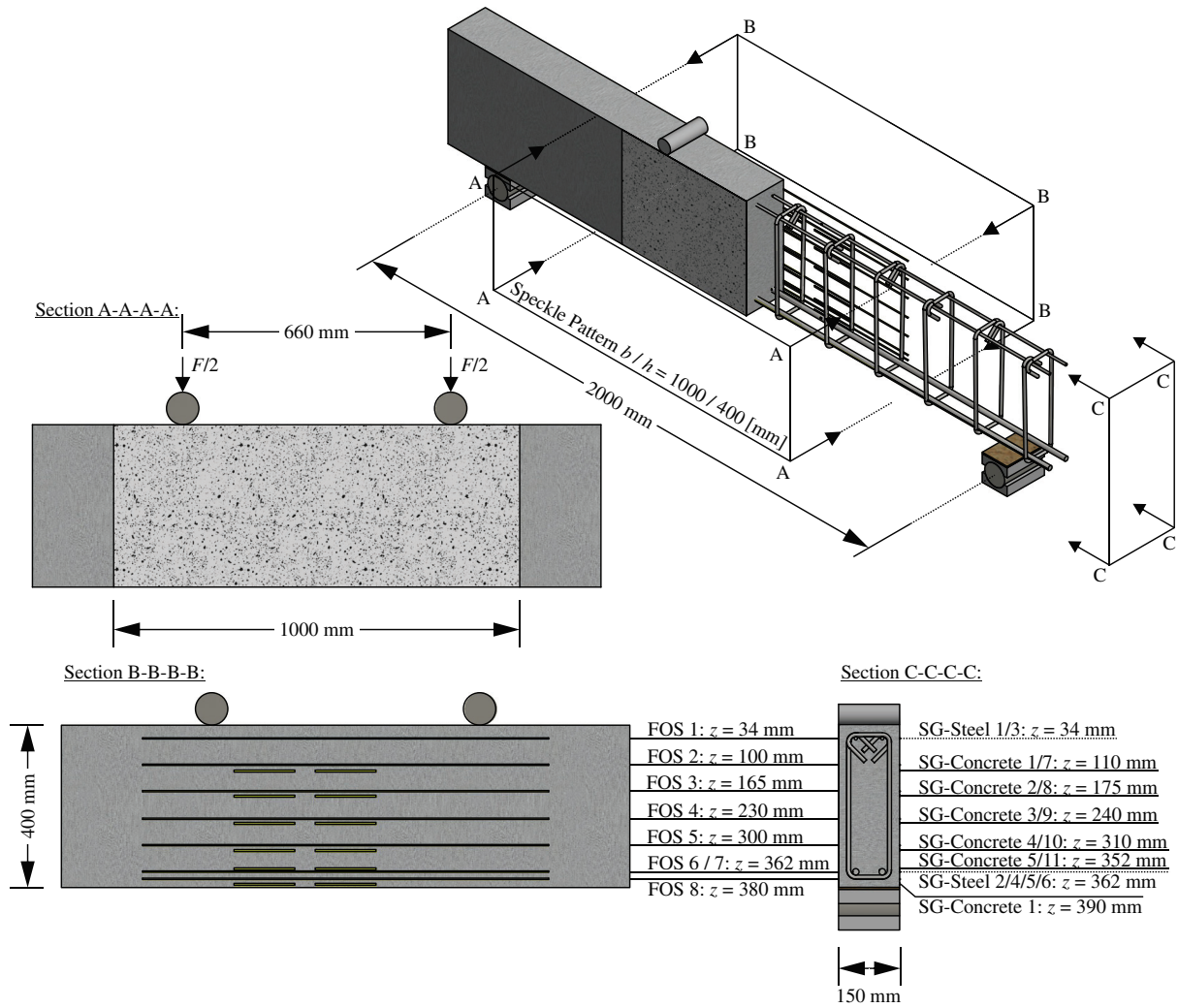
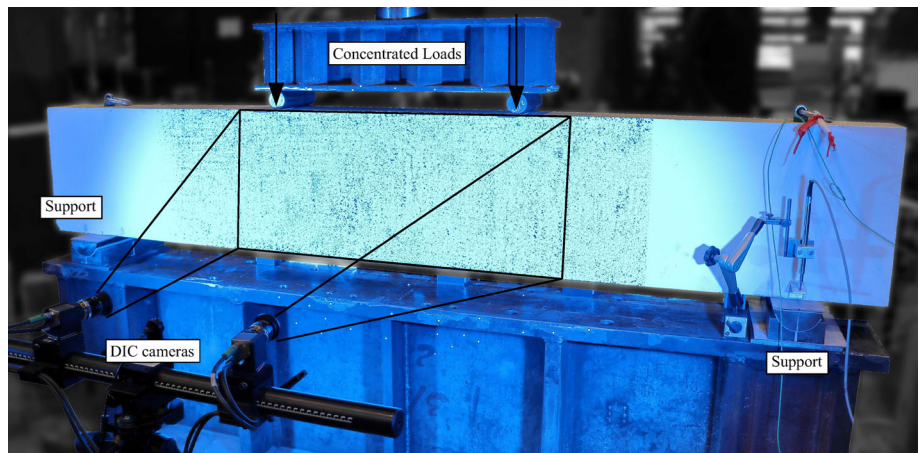


FIGURE 6 Test Set-Up of the Four-Point Bending Test (modified with reference to Clauß, 2020)

FIGURE 7 Front-Side of the Test Set-Up with the Cameras for DIC in the Foreground (modified with reference to Clauß, 2020)



(SDK), a quick-paced, automatized change among the eight channels is possible. This shortcoming is offset by the design of the load scenario. As pointed out earlier, the stepwise increasing load levels, which are held

constant for a short period of time, allow for each channel to be triggered at every load level. Such a progression leads to quasi-simultaneous measurement across all eight channels, that is, all eight FOS. Since creeping effects

within the RC beam cannot be avoided, the measurement of the first fiber was repeated at the end of the 8-channel succession on each load level to quantify these effects. As to the precise arrangement of the FOS, one sensor was attached in a notch along the reinforcement bar, while another seven FOS were attached distributed over the height of the surface of the test specimen (cf. Figure 6).

Moreover, conventional strain gauges were to be installed. In the set-up discussed here, a distinction must be made between strain gauges that are applied to the reinforcing steel on the one or to the concrete on the other hand. In this context, strain gauges with a length of 3 mm were used for measuring the strain of the reinforcement. In contrast, much longer strain gauges, measuring 100 mm in grid length, were used for measuring concrete strain. This distinction is necessary because the true strain state along the entire grid length is integrated into one strain value. In order to avoid deviations in recorded strain measurements caused by detection of fluctuating strain, attributable to the inhomogeneity of the concrete, a larger grid is used (cf. Figure 6).

### 3.2.3 | Results

Figure 8 shows strains recorded by FOS and strain gauges (Figure 8(a)), as well as DIC (Figure 8(b)). The unprocessed values produced by the FOS are illustrated in gray. In order to smooth out these highly fluctuating, scattered values, a stepwise robust linear regression was applied to the data points. Such a process always entails a loss of local information. Hence, the window length must be weighed against this loss of data. However, as depicted in Figure 8(a), the measured strains of the FOS and the strain gauges match well.

The imagery produced by DIC for a facet size of  $19 \times 19$  pixels =  $19^2$  pixel<sup>2</sup> and a load of 160 kN (Figure 8(b)) displays the alternating crack pattern of primary and secondary flexural cracks. In addition, flexural-shear cracks are indicated at the edges, while for the rest of the test specimen a mélange of neutral, tensile, and compressive strains appear to have occurred. However, as will be detailed further in the following, such scattered values result from measurement noise and therefore do not represent the true forces operating in the test specimen.

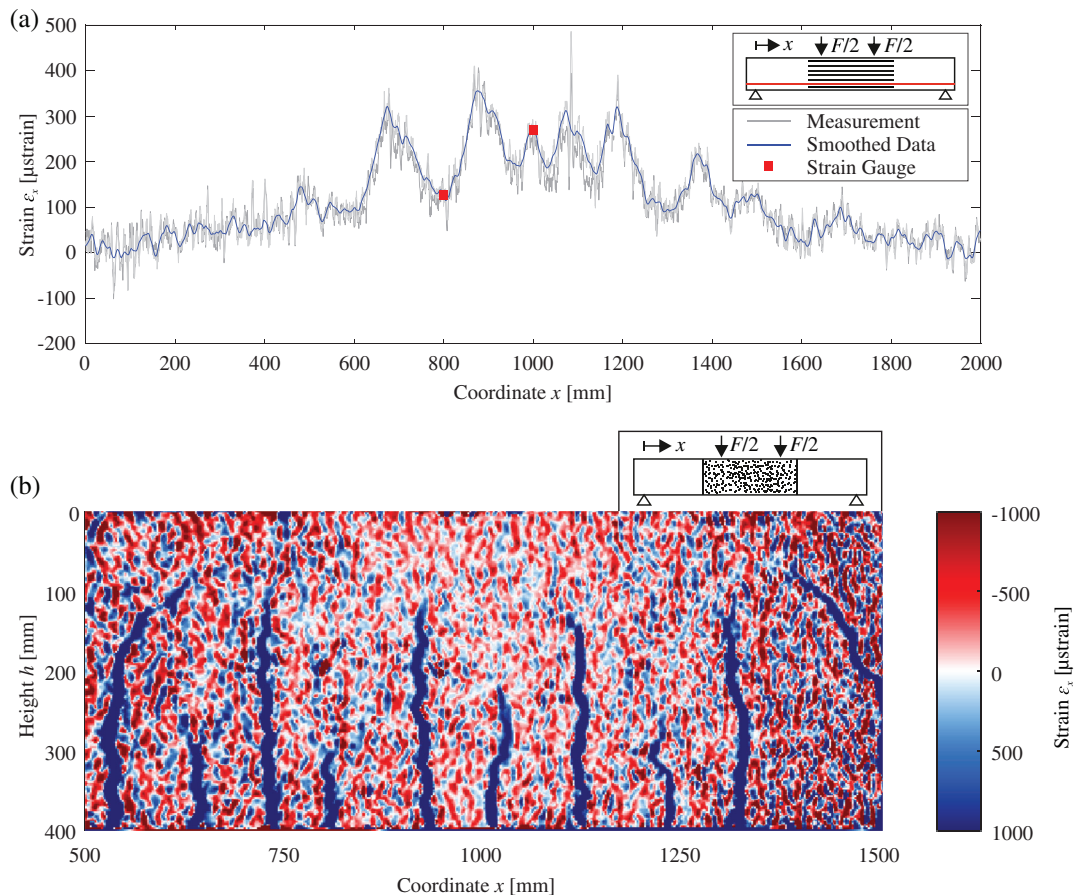


FIGURE 8 Strain Results from a) FOS and Strain Gauges as well as b) DIC at a Load of 160 kN (modified with reference to Clauß, 2020)

## 4 | COMPARISON OF STRAIN MEASUREMENT TECHNIQUES

### 4.1 | Assembly and application

#### *Strain gauges*

Since strain gauges are a measuring technique whose mode of operation is based on the change in electric resistance levels under changing external influences, protection against water ingress, for example, is a matter of course. Ex factory, SG are usually purchased fully assembled from the respective manufacturer. The measuring grid with the corresponding polyimide film is applied using a suitable adhesive—for steel applications, such as on reinforcing steel, for example, a cyanoacrylate has been proven to be adequate. In contrast to the application on steel, a two-component epoxy resin is used for concrete. This difference in the utilized adhesives can largely be attributed to the porosity of the concrete surface. A thin adhesive layer between the strain gauge and the measured object ensures that the force is transmitted mostly unaltered by the adhesive. More specialized variants of strain gauge technology also enable underwater measurements. Generally, however, they are usually covered with an aluminum foil, including a plasticine compound to protect it against, for example, mixing water.

#### *Fiber optic sensors*

As shown in Figure 9(a), the glass fiber of a FOS consists of a core, a cladding, and a coating. In order to splice different glass fibers together, the outer coating must be removed mechanically. In analogy to strain gauges, FOS can also be purchased fully assembled. However, it is also possible to assemble a FOS from the three components shown in Figure 9(b). For this purpose, the three components (pigtail, sensor fiber, and termination) are spliced together in the depicted order. The corresponding splice loci (ends spliced together utilizing an electric arc) are considered to be particularly brittle and are therefore

protected by a tube equipped with metal pin reinforcements.

Since FOS technology executes measurements of the Rayleigh component of the backscattered light spectrum, it is necessary to completely eject the emitted light from the core at the end of the sensor. To such ends, one aspect of the termination fiber's light transmission characteristics is exploited. Contrary to the sensor fiber, which is, in fact, specifically designed to do so, the termination fiber does transmit light inadequately when arranged in a loop with a small bend radius. The physical process underlying such behavior can be described as follows: the induced light beam within the termination fiber's core strikes the interface between the core and the surrounding cladding at an angle that prevents total reflection of the light and thus gradually channels the emitted light out. Therefore, the fiber of the termination is laid in short loops in order to ensure the complete ejection of the induced light.

In contrast to the application of a strain gauge to a concrete or steel surface, the previously introduced tests and the respective investigations (Chapter 3) indicated that the application of the AC2411 adhesive provides good results both for embedded reinforcing bars (see also Figure 10) and for the direct application to concrete surfaces. The employed adhesive (AC2411) solves the trade-off between measurement failures in certain areas (i.e., stiffer adhesive) and an excessive smoothing of the measured values (i.e., less stiff adhesive) well. However, this specific adhesive proves useful for applications of FOS in testing scenarios where the sensor is cast within the concrete specimen. If such direct contact is avoided (cf.<sup>39</sup>), the use of cyanoacrylate is the better choice due to its high stiffness and the associated accurate strain measurement. This knowledge can, therefore, be transferred analogously to steel component contexts. The absence of strain peaks on smallest areas, as it occurs in case of cracking of concrete, allows the advantageous use of cyanoacrylate. Among epoxy resins, AC2411 has proven to be the most useful adhesive.

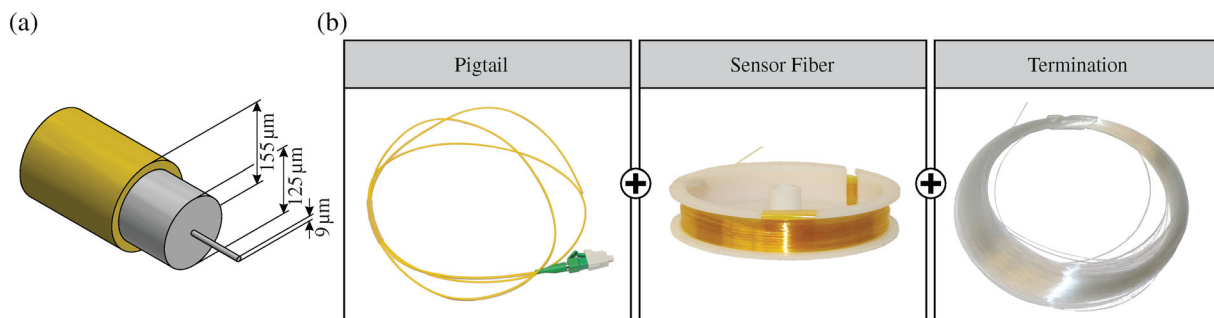


FIGURE 9 a) Glass Fiber Consisting of Core, Cladding, and Coating, b) Components of a FOS

At the onset of the experiment a reference measurement, for example, in a load-free scenario, is executed. Such result is employed as a comparative measurement to subsequent strain recordings (cf. Figure 2).

#### *Digital image correlation*

In contrast to the two measurement techniques described above, DIC does not require profound assembly or specific application of the measuring technology within or onto the test specimen. Instead, the distances between the cameras themselves, as well as the distance to the test specimen must be modified in accordance to the individual scenario's requirements. Moreover, the grain structure of the employed speckle pattern is pivotal and executed as follows. As depicted in Figure 11, the sample to be examined is first painted white, and then a black speckle pattern is applied. Upon said application, both the random arrangement of the speckle pattern (allowing for the retrieval of a section [facet] in different load scenarios via mathematical optimization) and the adequate distribution of individual speckles (preferably in a unique pattern of gray-scale pixels within the image section) are to be closely monitored.

Also, accurate positioning of the cameras, especially concerning the parallel arrangement of cameras' plane and measuring plane, surrounding lighting conditions, and, for example, possibly changing heat sources are of crucial importance.

## 4.2 | Accuracy and error evaluation

#### *Strain gauges*

As can be observed for the FOS (cf. ensuing segment), (uniaxial) strain gauges likewise only measure strain in one designated direction. Consequently, a small (unplanned) skew of the strain gauge (or the FOS) is more likely to occur when, for example, a rather small strain gauge is applied to a large reinforcement steel body. Here, applying the gauge in geometric accordance parallel to the body's longitudinal axis is a true challenge and may quickly result in angular errors. Due to the geometric dimensions of the object under test, however, this error is often difficult to quantify. An imprecise application can be avoided by using larger strain gauges

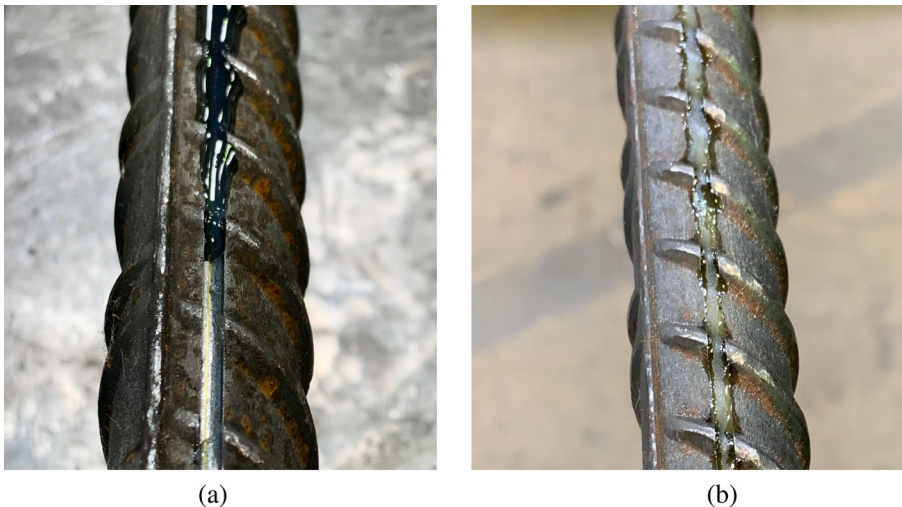


FIGURE 10 a) Partially and b) Completely Glued FOS into a Notch along a Rebar



FIGURE 11 Speckle Pattern and Cameras for DIC Strain Measurements

(cf. Figure 1). In doing so, manual application is facilitated, and the correct position can be best approximated optically. Inaccuracies that cannot be detected by the eye only engender slight angular errors leading to negligibly distorted results.

Equally difficult to evaluate is the correct amount of adhesive overall and below the sensor. If the adhesive layer is too thick, the strain can be spread, producing results described above.

In addition to measurement errors resulting, for example, from an inadequate application (such as an increased thickness of the adhesive, angle errors during the application, or improper insulation against moisture penetration), the following section focuses on measurement errors on the part of the respective measuring instrument. If negative influences are assumed, for example, self-heating of the strain gauge and a residual error due to exclusively linear temperature compensation, the zero point-related measurement error can be estimated at approx. 10–15  $\mu$ strain. Besides, there is measuring inaccuracy resulting from the measuring device itself as well as the tolerance within the strain gauges' k-factor. The non-zero point error can be estimated at 1%. It should be noted, however, that the context-relevant factors were calculated using conservative estimates.

A dispersion of the measured values around a constant value could be measured in tests on polished stainless-steel tension rods. A scattering of less than 1  $\mu$ strain was observed here (cf.<sup>39</sup>).

#### *Fiber optic sensors*

Similar to the observations made for strain gauges, measurement errors are also to be expected with FOS results stemming from, for example, an inadequate application within the test specimen (inappropriate adhesive layer or corrugated, non-linear application).

Furthermore, as discussed in Chapter 2, the measured frequency shift simultaneously depends on both strain and temperature.<sup>31</sup> The assessment of strain and temperature coefficient underlines that strain changes have a more significant influence on the frequency shift. When measuring mechanical strain and impact by an unexpected temperature, the latter influence is usually rather small. On the other hand, the recorded measurement values are strongly distorted when measuring temperature and an unexpected mechanical strain.

As stated in References 31 and 38 and depicted in Table 2, the measurement's repeatability, that is, the scattering of the measured values around a constant level, can be specified with  $\pm 20$   $\mu$ strain or  $\pm 5$   $\mu$ strain depending on the mode of operation. For the experiments elucidated here, the measurement mode with the smallest point distance of 0.65 mm was selected (repeatability  $\pm 20$   $\mu$ strain).

For the following testing scenarios, smaller point spacing and even more importantly the thereby decreased number of measurement failures is selected, despite the disadvantages of (1) lower measurement repeatability and (2) lower measurement frequency:

- for quasi-static tests,
- tests in which high fluctuations in the strain results are to be expected (such as measurements of steel strains in a concrete body or concrete strains),
- tests in which a high point-density in the results is necessary and
- tests where strains can be recorded, which exceed the repeatability many times over.

Accuracy of the strain measurement can be specified at  $\pm 25$   $\mu$ strain regardless of the selected mode of operation.

#### *Digital image correlation*

The advantage of DIC is constituted by the fact that measured results are not reliant on fixations such as adhesive or an improper misalignment of the sensor. Similar to both measurement methods discussed before, the generalization of an absolute measurement deviation or a measurement error is difficult to achieve with DIC. Here, variety of (environmental) variables influencing recordings produced via DIC, such as changing light or temperature conditions, or, for example, a deterioration of the imaging performance in the edge areas of an image, obstruct such generalized assertions. Furthermore, the results also depend on the generated information density. Significant factors in this context are the distance between the cameras and the object to be measured, as well as the resolution of the camera(s) used.

The load on the RC beam in the four-point bending test was increased sequentially in 5 kN steps. Approx. 30 pictures were taken with both cameras. For Figure 12 (below), the standard deviation (SD) of the strain on one load level was calculated. It is to be stressed that the SD and thus also the scattering of the measured values in the horizontal edge areas increase. On the other hand, an approximately constant SD along the vertical axis can be deduced.

Figure 12 juxtaposes SD values of measurements recorded by DIC for four different facet sizes (19<sup>2</sup>, 39<sup>2</sup>, 59<sup>2</sup>, and 100<sup>2</sup> pixel<sup>2</sup>). It is evident that the scattering decreases with increasing size of the facets. As was to be expected, increased facet size produces lower resolution. Such loss of information allows for less specific assertions on local deviations, that is, phenomena indicating local strain concentrations.

As stated before, the SD of the recorded behavior of different facets compared along the vertical axis remains

Mode of operation		High resolution	Extended length
Data acquisition rate	[Hz]	23.8	50
Maximum sensor length	[m]	10	20
Gauge length	[mm]	1.3	5.2
Gauge pitch	[mm]	0.65	2.6
Repeatability at zero strain	[ $\mu$ strain]	$< \pm 20$	$< \pm 5$
Repeatability across full strain range	[%]	$\pm 0.55$	$\pm 0.10$
Accuracy	[ $\mu$ strain]	$\pm 25$	$\pm 25$

TABLE 2 Modes of operation of the used fiber-optic device (ODiSI-B, Luna Inc.)

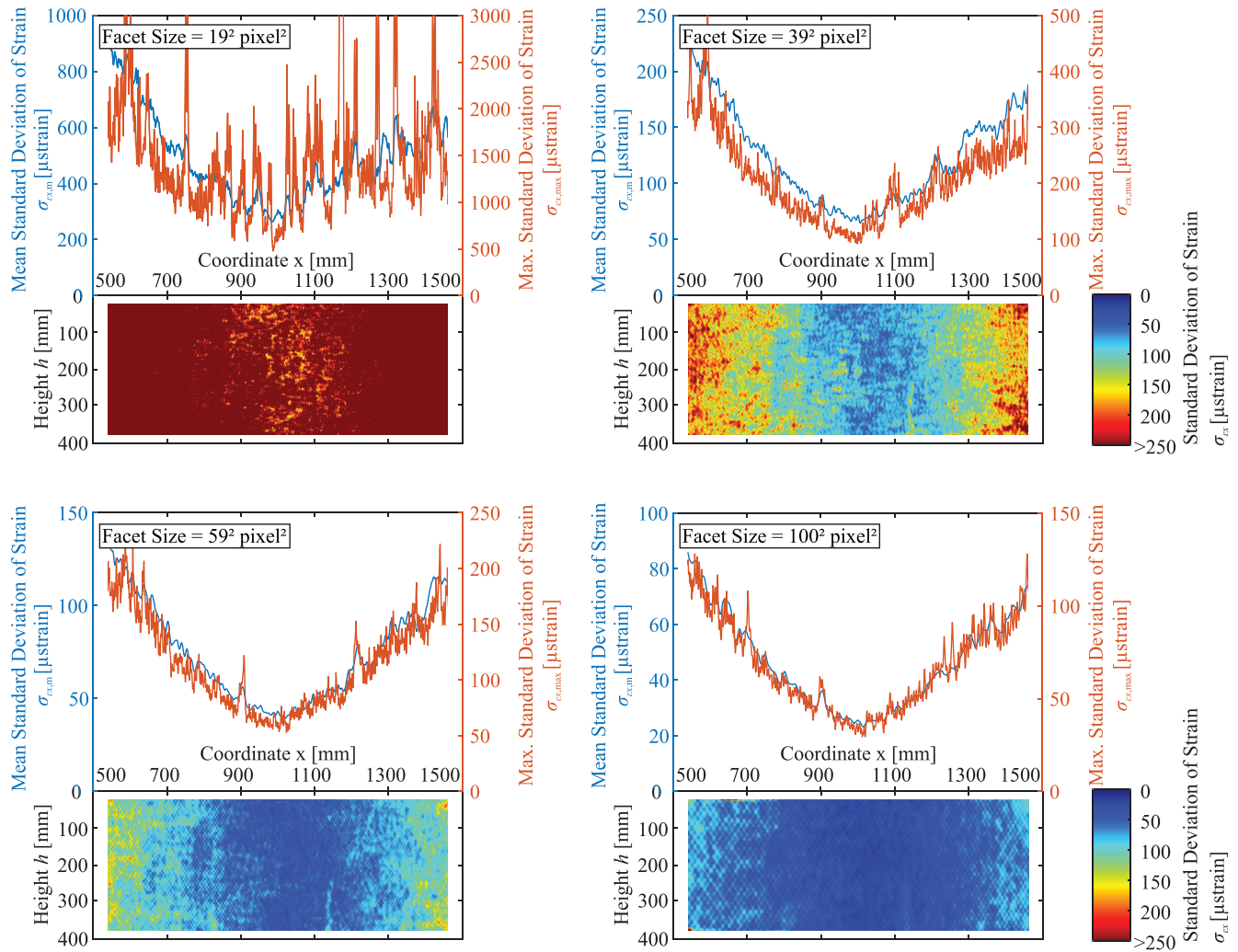


FIGURE 12 Spatial Standard Deviation from DIC Strain Measurements

very similar. The color schemes presented in Figure 12 clearly underscore this highly analogous state, for example, along the vertical axis in the edge areas. In this way, the SD can be averaged over the height (blue graph), or the maximum value (red graph) can be evaluated (Figure 12 above).

Table 3 compares different SD values (mean and max. SD of strain) from Figure 12 for the four facet sizes at the

center of the concrete beam, that is, at  $x = 1000$  mm. At this specific location, both mean (blue) and max. (red) SD graphs reach global minima. Since the two cameras employed here both focus on one facet at the true center of the recorded plane, that is,  $x = 1000$  mm;  $y = 200$  mm, the imagery generated here is of the highest repeatability possible—as discussed, the cameras' performance deteriorates toward the edge of the images. Thus, the DIC-

TABLE 3 Mean and max. SD of strain read from Figure 12 (top) for  $x = 1000$  mm

Facet size (pixel <sup>2</sup> )	Mean SD of strain $\sigma_{ex,m}$ ( $\mu$ strain)	Max. SD of strain $\sigma_{ex,max}$ ( $\mu$ strain)	$\sigma_{ex,m}/\epsilon_{cr} = \sigma_{ex,m}/100$ $\mu$ strain (–)	$\sigma_{ex,max}/\epsilon_{cr} = \sigma_{ex,max}/100$ $\mu$ strain (–)
19 <sup>2</sup>	300	500	3	5
39 <sup>2</sup>	75	150	0.75	15
59 <sup>2</sup>	40	60	0.4	0.6
100 <sup>2</sup>	25	35	0.25	0.35

recorded strain measurements and their SD not only allows for inferences on repeatability but also provides the basis for assessing the viability of different facet sizes for measuring concrete strain.

As initial cracking in concrete occurs at 100  $\mu$ strain, the ratio between said strain level and the (lowest) SD recorded in a facet ( $\sigma_{ex,m}/\epsilon_{cr} = \sigma_{ex,m}/100$   $\mu$ strain). If the ratio is = 1 or  $\gg 1$ , the facet is impracticable for measuring concrete tensile strain, if it is  $\ll 1$  it is suitable for doing so—values in between must be assessed individually. Here, regarding the issue of repeatability, the largest facets size of 100<sup>2</sup> pixel<sup>2</sup> offers the highest repeatability and, at least concerning this characteristic, outperforms the other variants. This is to be considered as a useful point of reference but cannot be fused into a general principle.

### Comparison

As discussed throughout this work, the test specimen was equipped with the three types of measuring techniques for repeated strain measurements—SG, FOS, and DIC. In order to contrast and critically discuss their characteristics, measurements produced by all three technologies were collected at a load level of  $F = 160$  kN—representing approx. 80% of the ultimate bearing capacity. Said load level ensures distinct strains. Figure 13 depicts six normal distributions generated via the parameters of the expected value  $\mu$ , as well as standard deviation  $\sigma$ . In this context, SGs, due to their performance as to repeatability (here:  $\sigma_{SG} = 0.23$   $\mu$ strain) and accuracy, as well as due to their long-established utilization are designated as the reference technology. That is, the parameter  $\mu_i$  for both FOS and the four facet sizes (DIC) is relative to the SG probability function: *related precision* =  $\mu_i - \mu_{SG}$ .

Here, 19<sup>2</sup> pixel<sup>2</sup> facet best approximates the reference SG value in terms of related precision ( $\mu_{FS19} = 16.16$   $\mu$ strain), while FOS, at 45.57  $\mu$ strain produce the largest *related precision*. However, it is crucial to be aware of the fact that all *related precision* values are indeed calculated using the SG parameter. Therefore, the *related precision* values illustrated in Figure 13 do not allow for simple, quantitative comparison among one another. Consequently,

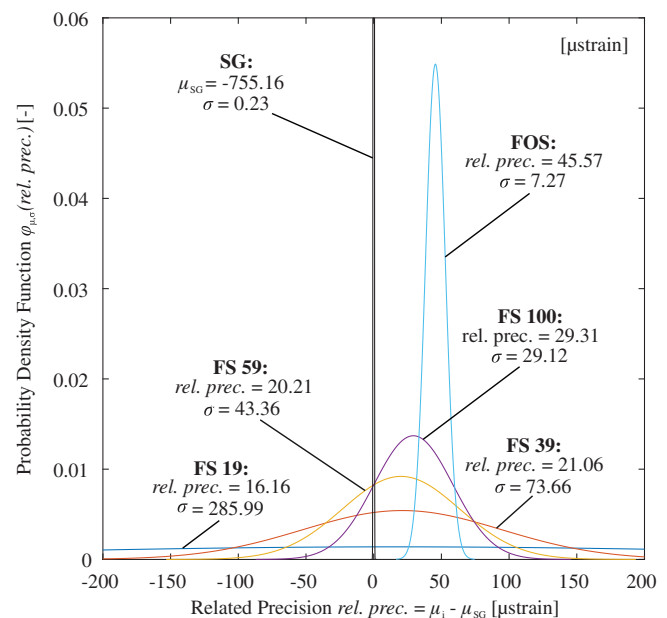


FIGURE 13 Idealized Distribution of the Measured Values at a load of  $F = 160$  kN in a Four-Point Bending Test

expected values ought to be compared in their absolute form:  $\mu_{FS19}/\mu_{SG} = 771.32/755.16 = 0.98$  and  $\mu_{FOS}/\mu_{SG} = 800.73/755.16 = 0.94$ . The ratios presented here nicely emphasize the negligible spread between the considered measurement techniques in terms of their produced accuracy (i.e.,  $\mu_i$ ). This insight prompts closer scrutiny of the repeatability performance of the three measurement techniques.

Having discussed the standard deviations for different facet sizes in DIC earlier (remarks on Figure 12 and Table 3), Figure 13 displays and contextualizes the three techniques' repeatability performance – and highlights the immense spread in this regard. While  $\sigma_{SG}$  clearly ranges top of the list at 0.25  $\mu$ strain,  $\sigma_{FOS}$  follows close behind at 7.27  $\mu$ strain. Again comparing this to the smallest facet of DIC (19<sup>2</sup> pixel<sup>2</sup>), the ratio is almost 40-fold ( $\sigma_{FS19} = 285.99$   $\mu$ strain). While all three types of measurement display relative similarity in terms of

accuracy (1 vs. 0.94), the spread in repeatability is much larger and requires a weighing of interests.

## 5 | CONCLUSIONS

In this work, the quality of strains in RC components recorded with different techniques is assessed. The applied techniques comprise common strain gauges for reference and more sophisticated technologies, namely FOS and DIC. Based on two test series on simple tension rods and a beam subjected to four-point bending general recommendations concerning device handling, sensor application (adhesive or non-contact), as well as material resilience, accuracy, repeatability, and measurement resolution on RC members are derived.

- Strain gauges exhibit the highest repeatability of strain readings ( $\sigma_{SG} < 1 \mu\text{strain}$ ) but with the lowest spatial resolution (0D). Since the accuracy of this long-established measurement technique is well-known and does not require further evaluation, it serves as a reference for the others. Severally repeated strain readings on constant load levels deliver stable means  $\mu_{SG}$  required to get and assess the performance of other techniques (*i*) by means of their relative precision ( $rel. prec. = \mu_{SG} - \mu_i$ ).
- In comparison FOS are less robust, quite tricky to apply and prone to damage during casting and testing but yield 1D quasi-continuous strains in concrete and steel along directed fibers. Especially a sound combination of fiber type and adhesive turns out decisive to get valuable strains. Testing of the tension rods revealed Polytec PT's AC2411 adhesive combined with a polyimide-coated fiber most promising for RC. With this combination testing in four-point bending yields a  $rel. prec. \approx 46 \mu\text{strain}$  along with a repeatability of  $\sigma_{FOS} \approx 7 \mu\text{strain}$ .
- With DIC technology, strain maps (2D) are calculated by correlating images recorded with two cameras. As a non-contact method external factors (heat sources, air currents, lighting conditions) and the installation of equipment (orientation of the cameras, quality of the spackle pattern) gain importance. Even more important is data smoothing driven by the facet size. With rising facet size from  $19^2$  to  $100^2$  pixel<sup>2</sup>, the repeatability is found increasing from  $\sigma_{DIC} \approx 286$  to  $29 \mu\text{strain}$ , while the relative precision is  $rel. prec. \approx 16$  to  $29 \mu\text{strain}$ .

Practically the  $rel. prec.$  of all alternatives is seen on an equivalent level and thus rated well-suited to record strain data in RC structures. Repeatability of the readings decreases with increasing dimensionality. As a rule of thumb, it decreases by one power per dimension.

If more dimensional measurement techniques are to be applied in a project, the installation effort truly rises, which can be justified with higher information density and spatial data. Nevertheless, the use of a few strain gauges for reference is strongly recommended and allows assessing measuring accuracies. Especially, repeated measurements on constant load levels enable to rate the robustness.

## ACKNOWLEDGMENTS

Financial support for this work was provided by the Deutsche Forschungsgemeinschaft (DFG, German Research Foundation) – Project number 398216472. This support is gratefully acknowledged.

Open access funding enabled and organized by Projekt DEAL.

## DATA AVAILABILITY STATEMENT

The data that support the findings of this study are available from the corresponding author upon reasonable request.

## ORCID

Felix Clauß  <https://orcid.org/0000-0001-5361-3255>

Mark Alexander Ahrens  <https://orcid.org/0000-0002-2337-1571>

Peter Mark  <https://orcid.org/0000-0003-1812-2148>

## REFERENCES

1. Heek P, Ahrens MA, Mark P. Incremental-iterative model for time-variant analysis of SFRC subjected to flexural fatigue. *Mater Struct.* 2017;50(62):1–15. <https://doi.org/10.1617/s11527-016-0928-z>.
2. Farrar CR, Worden K. An introduction to structural health monitoring. *Phil Trans R Soc A.* 2007;365:303–15. <https://doi.org/10.1098/rsta.2006.1928>.
3. Wenzel H. Health monitoring of bridges. New Jersey, USA: John Wiley & Sons; 2008.
4. Müller A, Sodeikat C, Schänzlin J, Knab F, Albrecht L, Groschup R, et al. The Gänstor bridge in Ulm – inspection, structural reanalysis, load test and bridge monitoring (die Gänstorbrücke in Ulm – Untersuchung, Probelastung und Brückenmonitoring). *Beton- und Stahlbetonbau.* 2019;115:164–78. <https://doi.org/10.1002/best.201900071>.
5. Wang X, Chakraborty J, Bassil A, Niederleithinger E. Detection of multiple cracks in four-point bending tests using the coda wave interferometry method. *Sensors.* 2020;20(1986):1–17. <https://doi.org/10.3390/s20071986>.
6. Löschmann J, Stötzel A, Dankmeyer U, Mark P. Gekoppelte Vermessungsstrategien für intelligente, digitale 3D-Stadtmodelle. *Messtechnik Bauwesen.* 2018;2018:6–11.
7. Löschmann J, Ahrens MA, Dankmeyer U, Ziem E, Mark P. Methods to reduce the partial safety factor concerning dead loads of existing bridges (Methoden zur Reduktion des Teilsicherheitsbeiwerts für Eigenlasten bei Bestandsbrücken).

- Beton- und Stahlbetonbau. 2017;112:506–16. <https://doi.org/10.1002/best.201700027>.
8. Sanio D, Löschmann J, Mark P, Ahrens MA. Measurements vs. analytical methods to evaluate fatigue of tendons in concrete bridges (Bauwerksmessungen versus Rechenkonzepte zur Beurteilung von Spannstahlermüdung in Betonbrücken). *Bautechnik*. 2018;95:99–110. <https://doi.org/10.1002/bate.201700092>.
  9. Obel M, Marwan A, Alsahly A, Freitag S, Mark P, Meschke G. Damage assessment concepts for urban structures during mechanized tunneling (Schadensbewertungskonzepte für innerstädtische Bauwerke bei maschinellen Tunnelvortrieben). *Bauingenieur*. 2018;93:482–91.
  10. Heek P, Tkocz J, Mark P. A thermo-mechanical model for SFRC beams or slabs at elevated temperatures. *Mater Struct*. 2018;51(87):1–16. <https://doi.org/10.1617/s11527-019-1340-2>.
  11. Sanio D, Mark P, Ahrens MA. Computation of temperature fields on bridges—implementation by means of spread-sheets (Temperaturfeldberechnung für Brücken). *Beton- und Stahlbetonbau*. 2017;112:85–95. <https://doi.org/10.1002/best.201600068>.
  12. Löschmann J, Clauß F, Mark P. Strengthening of reinforced concrete structures with temperature induction (Verstärken von Stahlbetontragwerken mit Temperaturinduktion). *Beton- und Stahlbetonbau*. 2020;115:746–57. <https://doi.org/10.1002/best.202000038>.
  13. Chen J, Yu Q, Cui X, Dong M, Zhang J, Wang C, et al. An overview of stretchable strain sensors from conductive polymer nanocomposites. *J Mater Chem C*. 2019;7:11710–30.
  14. Pan B, Tian L. Advanced video extensometer for non-contact, real-time, high-accuracy strain measurement. *Opt Express*. 2016;24:19082–93. <https://doi.org/10.1364/OE.24.019082>.
  15. D'Alessandro A, Meoni A, Ubertini F, Luigi Materazzi A. Strain Measurement in a Reinforced Concrete Beam Using Embedded Smart Concrete Sensors. In: di Prisco M, Menegotto M, editors. *Proceedings of Italian Concrete Days. ICD 2018. Lecture Notes in Civil Engineering. Volume 42*. Cham: Springer; 2018. [https://doi.org/10.1007/978-3-030-23748-6\\_22](https://doi.org/10.1007/978-3-030-23748-6_22).
  16. Lezgy-Nazargah M, Saeidi-Aminabadi S, Yousefzadeh MA. Design and fabrication of a new fiber-cement-piezoelectric composite sensor for measurement of inner stress in concrete structures. *Arch Civil Mech Eng*. 2019;19(2):405–16. <https://doi.org/10.1016/j.acme.2018.12.007>.
  17. Niederleithinger E, Wolf J, Mielentz F, Wiggenhauser H, Pirskaewetz S. Embedded ultrasonic transducers for active and passive concrete monitoring. *Sensors*. 2015;15:9756–72. <https://doi.org/10.3390/s150509756>.
  18. Tondolo, F.; Matta, E.; Quattrone, A.; Sabia, D. Experimental test on an RC beam equipped with embedded barometric pressure sensors for strains measurement. *Smart Mater Struct* 2019; 28(5):1–8. <https://doi.org/10.1088/1361-665X/ab1172>.
  19. Ge Y, Elshafie M, Dirar S, Middleton C. The response of embedded strain sensors in concrete beams subjected to thermal loading. *Construct Build Mater*. 2014;70:279–90. <https://doi.org/10.1016/j.conbuildmat.2014.07.102>.
  20. Fischer O, Thoma S, Crepez S. Distributed fiber optic sensing for crack detection in concrete structures (Quasikontinuierliche faseroptische Dehnungsmessung zur Rissdetektion in Betonkonstruktionen). *Beton- und Stahlbetonbau*. 2019a;114:150–9. <https://doi.org/10.1002/best.201800089>.
  21. Fischer O, Thoma S, Crepez S. Distributed fiber optic sensing for crack detection in concrete structures. *Civ Eng Des*. 2019b; 1:97–105. <https://doi.org/10.1002/cend.201900008>.
  22. Speck K, Vogdt F, Curbach M, Petryna Y. Fiber optic sensors for continuous strain measurement in concrete (Faseroptische Sensoren zur kontinuierlichen Dehnungsmessung im Beton). *Beton- und Stahlbetonbau*. 2019;114:160–7. <https://doi.org/10.1002/best.201800105>.
  23. Clauß F, Epple N, Ahrens MA, Niederleithinger E, Mark P. Comparison of experimentally determined two-dimensional strain fields and mapped ultrasonic data processed by coda wave interferometry. *Sensors*. 2020;20(4023):1–16. <https://doi.org/10.3390/s20144023>.
  24. Hoffmann, K. An introduction to stress analysis using strain gauges – the definitive work on strain gauge measurement. 2012.
  25. Kreger ST, Gifford DK, Froggatt ME, Soller BJ, Wolfe MS. High resolution distributed strain or temperature measurements in single- and multi-mode fiber using swept-wavelength interferometry. *Opt Fiber Sensors*. 2006;2006:1–4. <https://doi.org/10.1364/OFS.2006.TheE42>.
  26. Gifford, D. K.; Soller, B. J.; Wolfe, M. S.; Froggatt, M. E. Distributed fiber-optic temperature sensing using Rayleigh backscatter. 31st European Conference on Optical Communication 2005, <https://doi.org/10.1049/cp:20050584>
  27. Peters KJ, Inaudi D. Fiber optic sensors for assessing and monitoring civil infrastructures. *Sensor Technol Civil Infrastruct*. 2014;1: 121–158. <https://doi.org/10.1533/9780857099136.121>.
  28. Villalba S, Casas JR. Application of optical fiber distributed sensing to health monitoring of concrete structures. *Mech Syst Signal Process*. 2013;29:441–51. <https://doi.org/10.1016/j.ymssp.2012.01.027>.
  29. Engelbrecht, R. Fiber optic strain and temperature sensing: overview of principles. *AMA conferences 2017 – SENSOR 2017 and IRS<sup>2</sup>, Proceedings Sensor 2017, 2017*, 255–260. <https://doi.org/10.5162/sensor2017/B6.1>
  30. Distributed fiber optic sensing: temperature coefficient for polyimide coated low bend loss fiber, in the –40°C to 200°C range. Roanoke, VA, USA: Luna Innovations; 2014.
  31. Optical distributed sensor interrogator model ODiSI-B: User's guide; version 5.2.1; ODiSI-B software 5.2.0. Blacksburg, VA, USA: Luna Innovations; 2017.
  32. Sutton, M. A.; Orteu, J. J.; Schreier, H. *Image Correlation for Shape, Motion and Deformation Measurements – Basic Concepts, Theory and Applications*. Springer US, Boston, MA, 2009.
  33. Pan B, Qian K, Xie H, Asundi A. Two-dimensional digital image correlation for in-plane displacement and strain measurement: a review. *Meas Sci Technol*. 2009;20:062001.
  34. Chu TC, Ranson WF, Sutton MA. Applications of digital-image-correlation techniques to experimental mechanics. *Exp Mech*. 1985;25:232–44. <https://doi.org/10.1007/BF02325092>.
  35. Bruck HA, McNeill SR, Sutton MA, Peters WH. Digital image correlation using Newton-Raphson method of partial differential correction. *Exp Mech*. 1989;29:261–7. <https://doi.org/10.1007/BF02321405>.
  36. GOM. *GOM Testing Technical Documentation since V8 SR1: Basics of Digital Image Correlation and Strain Calculation; (GOM Testing Technische Dokumentation ab V8 SR1: Grundlagen der digitalen Bildkorrelation und Dehnungsberechnung); GOM GmbH: Braunschweig, Germany, 2016*.
  37. Winter, D. *Optische Verschiebungsmessung nach dem Objekttrasterprinzip mit Hilfe eines flächenorientierten Ansatzes*. Ph.D. Thesis, Technische Universität Carola-Wilhelmina zu Braunschweig, Braunschweig, Germany, 1993.

38. Konertz D, Löschmann J, Clauß F, Mark P. Fiber optic sensing of strain and temperature fields (Faseroptische Messung von Dehnungs- und Temperaturfeldern). *Bauingenieur*. 2019;94:60–167.
39. Konertz D, Kocur GK, Häusler F, Mark P. Longitudinal shear transmission of anchor channels into concrete—an experimental approach. *Struct Concr*. 2020;1–13. <https://doi.org/10.1002/suco.202000133>.

## AUTHOR BIOGRAPHIES



Felix Clauß  
Institute of Concrete Structures,  
Faculty of Civil and Environmental  
Engineering  
Ruhr University Bochum  
Bochum, Germany  
[felix.clauss@rub.de](mailto:felix.clauss@rub.de)



Mark Alexander Ahrens  
Institute of Concrete Structures,  
Faculty of Civil and Environmental  
Engineering  
Ruhr University Bochum  
Bochum, Germany  
[alexander.ahrens@rub.de](mailto:alexander.ahrens@rub.de)



Peter Mark  
Institute of Concrete Structures,  
Faculty of Civil and Environmental  
Engineering  
Ruhr University Bochum  
Bochum, Germany  
[peter.mark@rub.de](mailto:peter.mark@rub.de)

**How to cite this article:** Clauß F, Ahrens MA, Mark P. A comparative evaluation of strain measurement techniques in reinforced concrete structures—A discussion of assembly, application, and accuracy. *Structural Concrete*. 2021;1–16. <https://doi.org/10.1002/suco.202000706>